

# Monitoring Gold Nanorod Synthesis by Localized Surface Plasmon Resonance

Anneet Gulati,<sup>†</sup> Hongwei Liao,<sup>‡</sup> and Jason H. Hafner<sup>\*,†,‡</sup>

Department of Physics & Astronomy and Department of Chemistry, Rice University, Houston, Texas

Received: February 28, 2006; In Final Form: August 24, 2006

Surfactants can direct the growth of gold nanoparticles to create anisotropic structures in high yield by simple means, yet the exact roles of surfactants and other reactants are not entirely understood. Here we show that one can exploit the geometrical dependence of the localized surface plasmon resonant extinction spectrum of gold nanorods to monitor their synthesis kinetics. By using quantitative measurements of nanorod extinction cross sections, Gans' theory for the spectral extinction of prolate spheroids can be normalized to provide values for the nanorod length and diameter from extinction spectra measured during growth. The nanorod length growth rate was first observed at 0.15 nm/s and decayed during the growth reaction. The rate dependence on nanorod size did not correspond to any simple reaction-limited or diffusion-limited growth mechanisms.

## Introduction

Gold nanorods exhibit strong optical extinction at visible and near-infrared wavelengths which can be tuned by adjusting the nanorod length and diameter.<sup>1–5</sup> With recent advances in their high-yield synthesis,<sup>6,7</sup> stabilization,<sup>8–11</sup> and bioconjugation,<sup>8–10,12</sup> gold nanorods are an increasingly applied nanomaterial.<sup>9,13–21</sup> Gold nanorods can be produced by a simple seed-mediated, surfactant directed synthesis in which small gold nanoparticles (the seed) are injected into a stable Au ion growth solution that contains surfactant.<sup>5,22,23</sup> FTIR spectroscopy and thermogravimetric analysis suggest that the surfactant, cetyltrimethylammonium bromide (CTAB), forms a bilayer on the growing nanoparticle surface<sup>24</sup> that regulates the nanoparticle growth rate. Growth anisotropy is thought to occur due to variations in the surfactant binding to different crystal facets and surface defects. While several studies support this general mechanism,<sup>6,7,25–29</sup> many details are unclear, including the structure of the surfactant–gold interface, the role of AgNO<sub>3</sub>,<sup>30–33</sup> and the nature of the seed nanoparticles.<sup>32</sup> Other models have been put forward in which CTAB micelles carry Au ions and are preferentially directed to sites of high curvature on the seed, resulting in anisotropic growth.<sup>34</sup> The current understanding of nanorod synthesis is certainly hindered by the complexity of the reaction, but it also suffers from a general lack of methods to measure the microscopic reaction rates. Most kinetic studies to date have been based on either *ex situ* transmission electron microscopy (TEM) observations of the nanorod length and diameter or spectroscopic measurements of the plasmon resonance peak wavelength to estimate the nanorod aspect ratio.<sup>7,34,35</sup> Here we present a detailed analysis of the nanorod extinction spectrum during the synthesis reaction. We use Gans' theory, an extension of Mie theory for elongated nanoparticles, to gain a microscopic view of nanorod synthesis kinetics.

## Experimental Methods

**Nanorod Synthesis.** Nanorods were synthesized as reported previously,<sup>8</sup> based on high-yield methods of El-Sayed<sup>6</sup> and

Murphy.<sup>7</sup> A growth solution was prepared by adding 4.75 mL of 100 mM cetyltrimethylammonium bromide (CTAB), 0.2 mL of 10 mM HAuCl<sub>4</sub>, and 30  $\mu$ L of 10 mM AgNO<sub>3</sub> to a plastic tube. Next 32  $\mu$ L of 100 mM ascorbic acid was added, which turned the growth solution from yellow-brown to colorless. A seed solution was prepared by adding 250  $\mu$ L of 10 mM HAuCl<sub>4</sub> to 7.5 mL of 100 mM CTAB with gentle mixing. Then 600  $\mu$ L of ice cold 10 mM NaBH<sub>4</sub> was added to the seed solution, which caused the color to turn pale brown. Nanorod growth was carried out in 3 mL plastic cuvettes so that the spectral extinction could be monitored with a spectrophotometer (Ocean Optics USB2000). Next 9  $\mu$ L of seed was added to 3 mL of growth solution in the cuvette and extinction spectra were recorded every second. The final gold nanorod structure was confirmed by transmission electron microscopy (JEOL 2010), and is shown in Figure 1. Control growth experiments were carried out by using the same seed and growth solutions but under ambient lab illumination. TEM and post-growth spectral analysis confirmed that the extinction measurements had no observable effect on the final nanorod structure.

**Nanorod Concentration and Extinction Coefficient.** Nanorod solutions were PEGylated as described previously.<sup>36</sup> The CTAB was removed from the nanorod suspension by three rounds of centrifugation, decant, and resuspension with DI water. Glass coverslips were cleaned with piranha solution (3:1 H<sub>2</sub>SO<sub>4</sub>:H<sub>2</sub>O<sub>2</sub>) (**Warning:** piranha solution can react violently with organic substance, exercise extreme caution!), rinsed with DI water, and dried with a stream of nitrogen. The coverslips were then processed in an oxygen plasma cleaner for 1 min (PDC32G, Harrick Scientific). The coverslips were immersed in a 10% APTES solution in ethanol, v/v, for 10 min, rinsed with DI water, and dried with nitrogen. The coverslips were immersed in the PEGylated nanorod sample for 4 h, rinsed with DI water, and dried with nitrogen. This procedure resulted in submonolayer nanorod films with sufficient density to observe the nanorod LSPR extinction spectrum. The nanorod surface density ( $\rho$ ) was determined by atomic force microscopy and the absorbance maximum at the longitudinal plasmon resonance ( $A_{\text{film}}$ ) was measured in the spectrophotometer. Using Beer's law, one can determine the corresponding nanorod extinction

\* Address correspondence to this author. E-mail: hafner@rice.edu.

<sup>†</sup> Department of Physics & Astronomy.

<sup>‡</sup> Department of Chemistry.

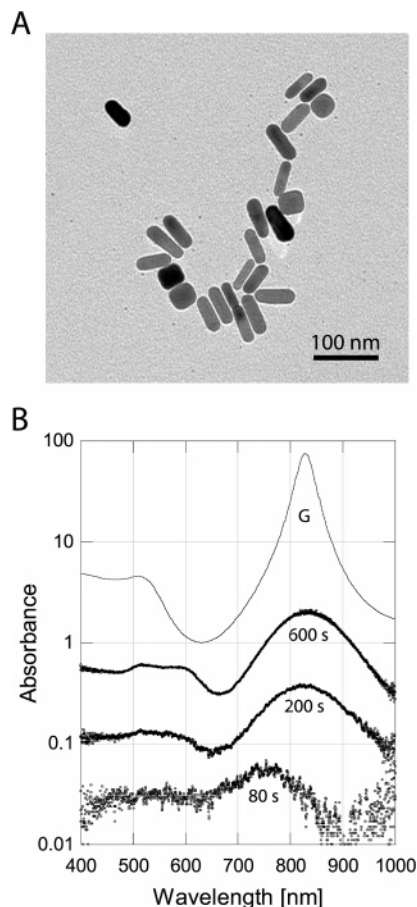


**Figure 1.** (A) Transmission electron micrograph of gold nanorods and (B) the extinction spectra recorded at various times during their synthesis, as well as a calculated extinction spectrum from Gans' theory.

cross section at the longitudinal plasmon resonance ( $\sigma$ ) from these parameters:

$$\sigma = (1/\rho_{\text{film}})(1 - 10^{-A_{\text{film}}}) \quad (1)$$

Given  $\sigma$ , the concentration of the nanorod solution ( $N$ ) can be determined from the absorbance maximum of the solution at the longitudinal plasmon resonance ( $A_{\text{soln}}$ ):

$$N = \frac{2A_{\text{soln}}}{\sigma d} \quad (2)$$

where  $d$  is the path length. The factor of 2 accounts for the random orientation of the nanorods in solution compared to the film, as previously described.<sup>8</sup> Since the nanorods were made by seed mediated growth, the nanorod concentration,  $N$ , determined after the synthesis was assumed equal to the concentration throughout the growth reaction.

**Calculation of Nanorod LSPR Spectra.** The LSPR of spheroidal metal nanoparticles can be calculated by Gans' theory, an extension of Mie theory, for spheroids:

$$\sigma = \frac{2\pi V \epsilon_m^{3/2} \sum_j \frac{(1/P_j)^2 \epsilon_2}{\left(\epsilon_1 + \frac{1 - P_j}{P_j} \epsilon_m\right)^2 + \epsilon_2^2}}{3\lambda} \quad (3)$$

where  $\sigma$  is the extinction cross section,  $V$  is the nanoparticle volume,  $\epsilon_m$  is the dielectric constant of the medium, and  $\epsilon_1$  and  $\epsilon_2$  are the real and imaginary components, respectively, of the

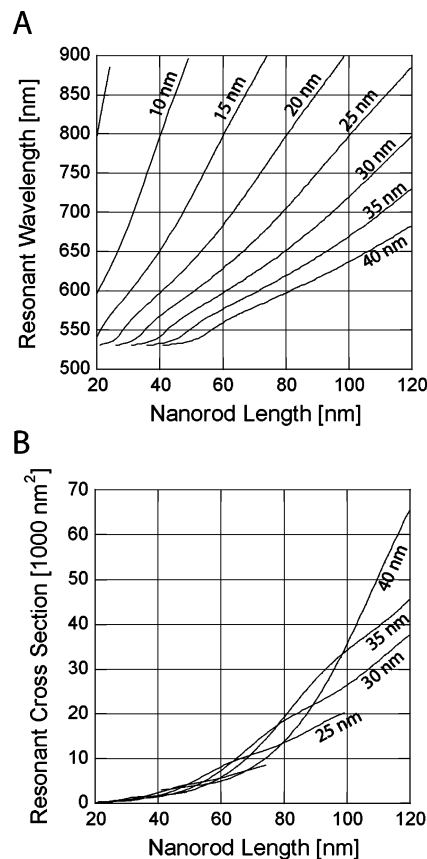


**Figure 2.** The longitudinal plasmon resonant wavelength (A) and cross section (B) for gold nanorods calculated by Gans' theory. The labels on the lines indicate the nanorod diameter.

dielectric function of the metal.<sup>1,2</sup> This expression is derived in the dipole approximation and is similar to that for spherical nanoparticles.  $P_j$  represent depolarization factors along the three Cartesian axes to account for anisotropic particle shape. By using the measured dielectric function of gold,<sup>37</sup> this theory has been demonstrated to *qualitatively* describe the LSPR spectra of gold nanorods, including the observed red-shift of the longitudinal plasmon band with increasing nanoparticle aspect ratio and with increasing dielectric constant of the medium.<sup>1,2</sup> For this study, the nanorod spectra were modeled by treating them as prolate spheroids for which the semimajor radii ( $a$ ) and the semiminor radii ( $b$ ) were set equal to half the nanorod length ( $l$ ) and half the nanorod diameter ( $d$ ), respectively. The prolate spheroid volume was used:  $V = 4\pi a^2 b/3$ . The dielectric medium was assumed to be water ( $n = 1.33$ ).

**Numerical Determination of Nanorod Structure from the LSPR Spectrum.** Nanorod spectra were calculated as described above for all nanorods with diameters,  $d$ , ranging from 3 to 40 nm and lengths,  $l$ , from 20 to 120 nm, but limited to those with an aspect ratio between 1 and 5. The calculations were carried out at 1 nm intervals, yielding 2435 spectra in this ( $l, d$ ) nanorod space. These Gans' theory spectra were analyzed to determine their longitudinal plasmon resonant cross section,  $\sigma_G$ , and their longitudinal plasmon resonant wavelength,  $\lambda_G$ . All values were normalized (see Results and Discussion section) to those calculated for the  $l = 50$  nm,  $d = 15$  nm nanorod. Subsets of the prenormalized results are displayed in Figure 2.

The experimental extinction spectra were similarly analyzed to determine their longitudinal plasmon resonant wavelength,  $\lambda_{\text{meas}}$ , and absorbance,  $A_{\text{meas}}$ . The  $A_{\text{meas}}$  were converted to longitudinal plasmon resonant cross sections,  $\sigma_{\text{meas}}$ , using eq 2, given the nanorod concentration,  $N$ , determined from the film

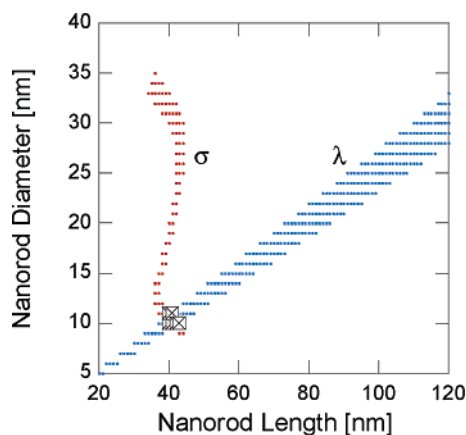


**Figure 3.** Method of nanorod length and diameter determination from the extinction spectra. The observed maximum wavelength (blue,  $\lambda$ ) gives one set of potential ( $l, d$ ) nanorods, and the maximum cross section (red,  $\sigma$ ) gives another. The union of the sets, designated by boxes, is averaged to determine the nanorod structure.

measurements. The measured values were normalized to the known values for the  $l = 50$  nm,  $d = 15$  nm nanorod:  $840 \text{ nm}^2$  cross section and  $755$  nm wavelength.<sup>36</sup>

To determine structural parameters from a measured spectrum, the normalized  $\lambda_{\text{meas}}$  was compared to the normalized  $\lambda_{\text{G}}$  for all nanorod structures. Those ( $l, d$ ) nanorods that fell within 5% of the measured value were collected as a set of candidate nanorod structures. Next, the normalized  $\sigma_{\text{meas}}$  was compared to the normalized  $\sigma_{\text{G}}$  for all nanorod structures, and those that fell within 2% were collected. To determine the nanorod structure for that spectrum, the intersection of these two sets was found, and the lengths and diameters of the nanorods in the intersection were averaged. The procedure is shown graphically in Figure 3. This procedure was applied to all spectra from a growth experiment to determine the nanorod length and diameter during the course of the nanorod synthesis.

## Results and Discussion

Nanorod synthesis was monitored from the initial injection of the seed solution. As seen in Figure 1b, a reliable nanorod spectrum was observed after about 80 s. The peak then increased in height, as one would expect for a solution of growing nanorods. A plot of the nanorod extinction spectrum from Gans' theory for an  $l = 50$  nm,  $d = 15$  nm nanorod in water is also shown to demonstrate the similarity to the measured spectra.  $\sigma_{\text{meas}}$  and  $\lambda_{\text{meas}}$  were chosen as the experimental parameters from which to derive the nanorod length and diameter. Figure 2 shows how these parameters are predicted to depend on  $l$  and  $d$  by Gans' theory. These plots are subsets of the full nanorod dataset described in the Methods section. Figure 2a displays  $\lambda_{\text{G}}$  as a function of nanorod length for different diameters. The linear dependence on length is expected since the longitudinal resonance red-shifts proportional to the nanorod aspect ratio ( $l/d$ ).<sup>1,2</sup> Figure 2b demonstrates that  $\sigma_{\text{G}}$  increases rapidly with length, but is largely insensitive to diameter. This is in contrast to the Mie theory prediction that extinction cross sections are proportional to nanoparticle volume in the dipole limit, which would imply strong diameter dependence for the nanorod spectra. However, the longitudinal resonance from Gans' theory is due to dipole excitation along the nanorod length, so only this dimension strongly affects the extinction cross section.

Gans' theory has been shown to accurately predict the dependence of  $\lambda_{\text{meas}}$  on nanorod geometry and local dielectric environment.<sup>1,2</sup> However, it cannot quantitatively predict  $\lambda_{\text{meas}}$

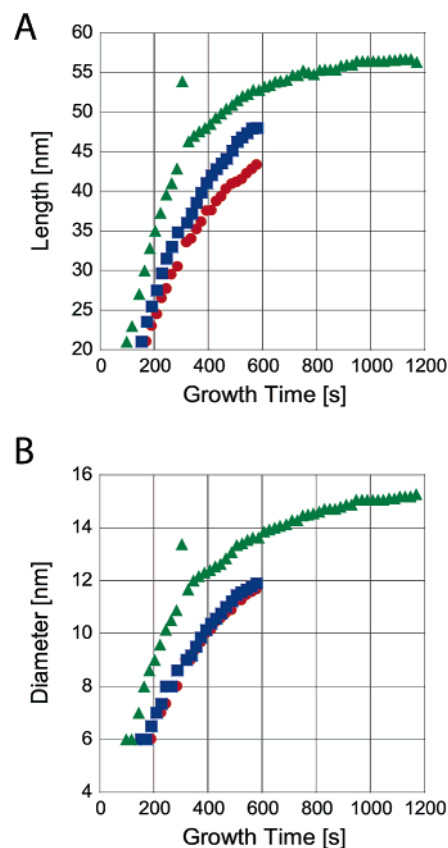


**Figure 4.** Gold nanorod length (A) and diameter (B) calculated for three separate growth experiments.

for a given  $l, d$ , and  $\epsilon_m$ .  $l$  and  $d$  are often measured by electron microscopy while  $\epsilon_m$  is adjusted to attain an accurate fit. In addition, one would not expect  $\sigma_{\text{G}}$  to be accurate since the nanorods are not prolate spheroids.<sup>21,38</sup> A quantitative numerical model is achieved here by normalizing  $\lambda_{\text{G}}$  and  $\sigma_{\text{G}}$  to the values measured for a specific nanorod structure. Therefore, our numerical technique only uses Gans' theory to capture the dependence of the nanorod spectra on geometry and environment. We recently described a method to make quantitative extinction cross section measurements based on the spectral extinction of submonolayer films of nanorods.<sup>36</sup> With the films, the number of nanorods contributing to the extinction can be measured by atomic force microscopy, enabling one to determine a quantitative extinction cross section. Nanorods with 50 nm length and 15 nm diameter had a peak wavelength of 755 nm and an extinction cross section of  $840 \text{ nm}^2$ . These measurements are in excellent agreement with those recently reported by an independent method.<sup>31</sup> All  $\lambda_{\text{meas}}$  and  $\sigma_{\text{meas}}$  were normalized to these values. The normalized experimental and calculated values can then be compared to quantitatively determine the structure from the spectrum.

Figure 4 presents the length and diameter as a function of growth time for three nanorod synthesis experiments as determined by the method described above and illustrated in Figure 3. The nanorods were first detected at a diameter of 6 nm and length of 20 nm. The two 600 s experiments were carried out with the same seed and growth solutions. The longer synthesis, which follows the entire growth reaction, was carried out with a separate but identical preparation. TEM analysis of the resulting nanorods (seen in Figure 1a) yields an average length of 56 nm, which matches that determined by the spectroscopic method, thus validating the rescaling of Gans' theory by using a measured extinction cross section and wavelength. However,

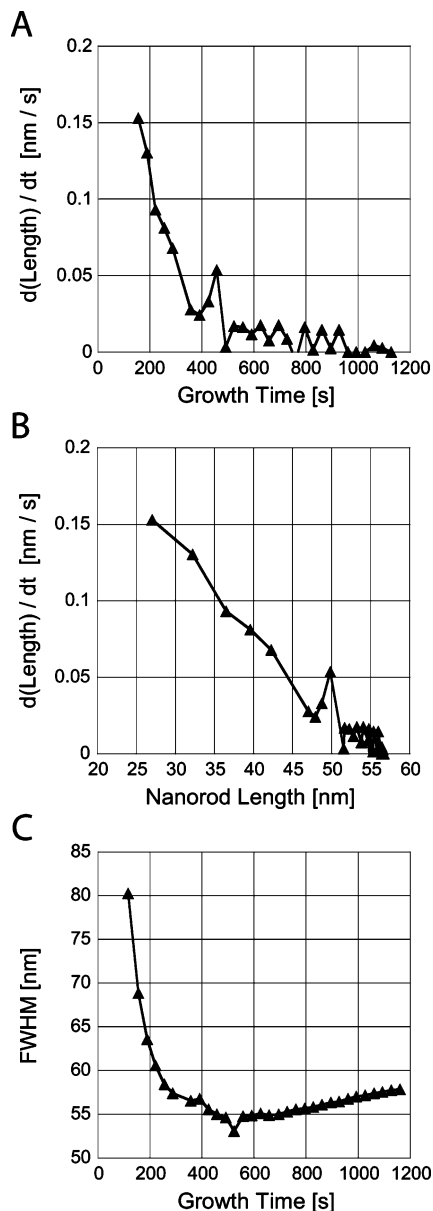


**Figure 5.** Analysis of the nanorod growth rates. The length growth rate dependence is plotted versus growth time (A) and nanorod length (B) for the long growth experiment in Figure 4. The fwhm of the fitted spectra (C) reveals a narrowing of the size distribution.

the spectroscopic method apparently underestimates the final diameter. Figure 4b suggests a final diameter of 15 nm while the TEM analysis yielded an average diameter of 19 nm. This may not be surprising since the spectroscopic method is based entirely on the longitudinal plasmon resonance. Recent advances in accurate calculations of nanorod spectra may be used to improve the analysis methods presented here.<sup>21,38</sup>

Nanoparticle growth rates were calculated from the data in Figure 4a. The length growth rate versus growth time is plotted in Figure 5a. The initial length rate of 0.15 nm/s decreases to near zero during the initial growth stage. Supporting evidence for the decelerating growth rate is given in Figure 5c, which displays the observed fwhm of the nanorod extinction spectra throughout the growth reaction. Single nanorods of this size have fwhm of approximately 50 nm,<sup>39</sup> so the larger values represent the heterogeneity in the nanorod ensemble. The decrease in size distribution indicates a growth rate that slows with increasing nanoparticle size.<sup>40</sup> Nanorod synthesis kinetics under identical conditions has been studied by TEM analysis

at various stages of growth.<sup>7</sup> In that report, length measurements at 1, 5, 10, and 15 min indicated a constant initial growth rate of only 0.02 nm/s. Although this appears to be a significant discrepancy, note that the TEM method provides much fewer measurements per unit time with significant error bars. In fact, the TEM data in that report are entirely consistent with an initial growth rate of 0.15 nm/s that trends toward zero as revealed here with faster time resolution and more accurate size measurements. TEM analysis of the kinetics can be improved by arresting the growth with sodium sulfide at various times before deposition onto a grid.<sup>35</sup> Qualitative kinetics was analyzed for similar growth conditions with this method, but the focus was on the longer term (>900 s) shape changes rather than the initial growth.

Nanoparticle growth generally occurs by diffusion of monomer (in this case Au ion) to a particle and then reaction with the surface. Either of the steps can be rate limiting, resulting in diffusion- or reaction-limited growth. If CTAB forms a bilayer on the nanorod surface to regulate the rate of reduction of Au ions as hypothesized, nanorod growth should be reaction-limited. Following Sugimoto, the rate law is:

$$\frac{dr}{dt} = kV_m(C_b - C_e) \quad (4)$$

where  $k$  is a first-order rate constant,  $V_m$  is the molar volume of gold,  $C_b$  is the bulk monomer concentration, and  $C_e$  is the solubility of the nanoparticle.<sup>40</sup> In the simple case of an excess of monomers (constant  $C_b$ ) and ignoring the Gibbs–Thomson effect (constant  $C_e$ , see below), reaction-limited growth results in a constant nanoparticle growth rate, which is clearly not observed in Figure 5. The observed deceleration of the growth could be due to depletion of Au ion monomers. However, given the nanorod extinction coefficient and the measured absorbance, the  $\text{Au}^0$  concentration of the final nanorod solution is in the nanomolar range, while both Au and Ag ions are present at micromolar concentrations in the growth solution. This significant excess of monomers suggests that growth is not slowed due to a lack of Au ions. A similar conclusion was drawn from an analysis of the total gold concentration in nanorod solutions by inductively coupled plasma atomic emission spectroscopy (ICP).<sup>31</sup> Alternatively, the decaying growth rate could suggest (1) a diffusion-limited reaction or the influence of the Gibbs–Thomson effect on (2) diffusion- or (3) reaction-limited growth.<sup>40</sup> The Gibbs–Thomson effect accounts for the size-dependent surface energy of the nanoparticle and alters the growth kinetics. Each of these three models predicts a unique dependence of the growth rate on nanoparticle size. However, none of the models match the linear size dependence observed here and plotted in Figure 5b.

These direct observations of the size dependent growth rate could help elucidate the mechanism of surfactant directed growth of gold nanoparticles. For example, in one model of nanorod growth the CTAB bilayer encapsulates the nanorods and regulates the rate of Au ion reduction since the charged species must pass through the hydrophobic interior of the bilayer. Selective absorption of the CTAB bilayer to different crystal facets and defects is then thought to cause growth anisotropy. Essentially, the formation of a more ordered CTAB bilayer along the nanorod sides relative to a disordered, or perhaps nonexistent, bilayer on the nanorod ends allows more rapid influx of Au ions to the ends. Perhaps the curvature of the bilayer, which would follow the curvature of the growing nanorod, also affects the bilayer order and therefore the Au ion permeation rate.<sup>41</sup> This would be equivalent to a size dependent rate constant,  $k$ ,

in eq 4. Such a model may better fit the data in Figure 5b rather than the asymptotic expressions derived from the Gibbs–Thomson effect.<sup>40</sup> Alternatively, it has also been suggested that the CTAB micelles regulate nanorod growth by acting as a carrier of Au ions during the reaction. The CTAB micelles are selectively drawn to the nanorod tips due to the enhanced electric field at regions of high curvature. Such a model would certainly predict a size dependent growth rate that could be compared to the data in Figure 5b.

## Conclusion

Here we have demonstrated a simple spectroscopic method to determine the microscopic length and diameter of gold nanorods during synthesis by comparing their plasmon resonant extinction spectra to those calculated by Gans' theory for prolate spheroids. Nanorod length and diameter were monitored to follow the kinetics of seed mediated, surfactant directed gold nanorod synthesis. The nanorod structure could be detected and analyzed by extinction for sizes as small as 6 nm diameter and 20 nm length. In contrast to constant growth rates from TEM observations, we find that the nanorod length rate decelerates throughout the initial growth phase. The size dependence of the growth rate did not follow simple reaction-limited or diffusion-limited growth kinetics.

**Acknowledgment.** The authors acknowledge the Robert A. Welch Foundation for support (Grant no. C-1556).

## References and Notes

- Link, S.; Mohamed, M.; El-Sayed, M. *J. Phys. Chem. B* **1999**, *103*, 3073.
- Link, S.; El-Sayed, M. A. *J. Phys. Chem. B* **2005**, *108*, 11876.
- Foss, C.; Hornyak, G.; Stockert, J.; Martin, C. *J. Phys. Chem.* **1994**, *98*, 2963.
- Yu, Y.-Y.; Chang, S.-S.; Lee, C.-L.; Wang, C. R. C. *J. Phys. Chem. B* **1997**, *101*, 6661.
- Jana, N. R.; Gearheart, L.; Murphy, C. J. *J. Phys. Chem. B* **2001**, *105*, 4065.
- Nikoobakht, B.; El-Sayed, M. A. *Chem. Mater.* **2003**, *15*, 1957.
- Sau, T. K.; Murphy, C. J. *Langmuir* **2004**, *20*, 6414.
- Liao, H.; Hafner, J. *Chem. Mater.* **2005**, *17*, 4636.
- Takahashi, H.; Niidome, Y.; Yamada, S. *Chem. Commun.* **2005**, 2247.
- Takahashi, H.; Niidome, Y.; Niidome, T.; Kaneko, K.; Kawasaki, H.; Yamada, S. *Langmuir* **2006**, *22*, 2.
- Thomas, K. G.; Barazzouk, S.; Ipe, B. I.; Joseph, S. T. S.; Kamat, P. V. *J. Phys. Chem. B* **2004**, *108*, 13066.
- Cassell, K. K.; Wilson, J. N.; Bunz, U. H.; Murphy, C. J. *J. Am. Chem. Soc.* **2003**, *125*, 13914.
- Wang, H.; Huff, T. B.; Zweifel, D. A.; He, W.; Low, P. S.; Wei, A.; Cheng, J.-X. *Proc. Natl. Acad. Sci. U.S.A.* **2005**, *102*, 15752.
- Sönnichsen, C.; Alivisatos, A. P. *Nano Lett.* **2005**, *5*, 301.
- Li, C. Z.; Male, K. B.; Hrapovic, S.; Luong, J. H. T. *Chem. Commun.* **2005**, 3924.
- Berry, V.; Gole, A.; Kundu, S.; Murphy, C. J.; Saraf, R. F. *J. Am. Chem. Soc.* **2005**, *127*, 17600.
- Rex, M.; Hernandez, F. E.; Carniglia, A. D. *Anal. Chem.* **2006**, *78*, 445.
- Huang, X.; El-Sayed, I. H.; Qian, W.; El-Sayed, M. A. *J. Am. Chem. Soc.* **2006**, *128*, 2115.
- Hu, X. G.; Cheng, W. L.; Wang, T.; Wang, Y. L.; Wang, E. K.; Dong, S. J. *J. Phys. Chem. B* **2005**, *109*, 19385.
- Sudeep, P. K.; Shibu, S. T.; Thomas, K. G. *J. Am. Chem. Soc.* **2005**, *127*, 6516.
- Alekseeva, A. V.; Bogatyrev, V. A.; Dykman, L. A.; Khlebtsov, B. N.; Trachuk, L. A.; Melnikov, A. G.; Khlebtsov, N. G. *Appl. Opt.* **2005**, *44*, 6285.
- Jana, N. R.; Gearheart, L.; Murphy, C. J. *Adv. Mater.* **2001**, *13*, 1389.
- Jana, N. R.; Gearheart, L.; Murphy, C. J. *Chem. Mater.* **2001**, *13*, 2313.
- Nikoobakht, B.; El-Sayed, M. A. *Langmuir* **2001**, *17*, 6368.
- Johnson, C. J.; Dujardin, E.; Davis, S. A.; Murphy, C. J.; Mann, S. *J. Mater. Chem.* **2002**, *12*, 1765.
- Gao, J. X.; Bender, C. M.; Murphy, C. J. *Langmuir* **2003**, *19*, 9065.
- Liao, H. W.; Hafner, J. H. *J. Phys. Chem. B* **2004**, *108*, 19276.
- Gai, P. L.; Harmer, M. A. *Nano Lett.* **2002**, *2*, 771.
- Wei, Z. Q.; Zamborini, F. P. *Langmuir* **2004**, *20*, 11301.
- Wu, H. Y.; Chu, H. C.; Kuo, T. J.; Kuo, C. L.; Huang, M. H. *Chem. Mater.* **2005**, *17*, 6447.
- Orendorff, C. J.; Murphy, C. J. *J. Phys. Chem. B* **2006**, ASAP.
- Liu, M.; Guyot-Sionnest, P. *J. Phys. Chem. B* **2005**, *109*, 22192.
- Chen, H. M.; Peng, H. C.; Liu, R. S.; Asakura, K.; Lee, C. L.; Lee, J. F.; Hu, S. F. *J. Phys. Chem. B* **2005**, *109*, 19553.
- Perez-Juste, J.; Liz-Marzan, L. M.; Carnie, S.; Chan, D. Y. C.; Mulvaney, P. *Advan. Funct. Mater.* **2004**, *14*, 571.
- Zweifel, D. A.; Wei, A. *Chem. Mater.* **2005**, *17*, 4256.
- Liao, H. W.; Hafner, J. H. *Chem. Mater.* **2005**, *17*, 4636.
- Johnson, P. B.; Christy, R. W. *Phys. Rev. B* **1972**, *6*, 4370.
- Prescott, S. W.; Mulvaney, P. *J. Appl. Phys.* **2006**, *99*.
- Sönnichsen, C.; Franzl, T.; Wilk, T.; von Plessen, G.; Feldmann, J. *Phys. Rev. Lett.* **2002**, *88*, 077402.
- Sugimoto, T. *Adv. Colloid Interface Sci.* **1987**, *28*, 65.
- Heerklotz, H. *Biophys. J.* **2001**, *81*, 184.